

Influence of 4D Data Assimilation inside the PBL for High Resolution Multiscale Simulations using WRF-LES in Real Complex Terrain

Pablo Cárdenas¹

Alex Flores^{2*}

¹Universidad Técnica Federico Santa María. Departamento de Ing. Mecánica. Valparaíso, Chile.

Email: pablo.cardenasz@alumnos.usm.cl

²Universidad Técnica Federico Santa María. Departamento de Ing. Mecánica. Valparaíso, Chile.

Email: alex.floresm@usm.cl

*Corresponding Author

Abstract: In order to develop a reliable tool to estimate the wind behavior in localized areas, a novel methodology that considers fields measurements at surface level was tested for multi-scale atmospherics simulations. Specifically, the WRF software was used to perform real simulations at very high resolution, i.e. mesh sizes up to 2m, through nested domains and the incorporation of non-native databases for orography and land use category. In the finer domains, the PBL parameterization was turned off and a 1.5TKE LES turbulence model was used. Finally, measured data was incorporated in the innermost domain through a 4D data assimilation system to correct the numerical deviations every 10 minutes in the first 6 hours of simulation. Five experiments are presented in two separate scenarios: (I) Høvsøre (quasi-flat terrain with neutral stratification) in which the DA was accomplished through a single-point mast measurement located at the domain center and (II) Bolund (complex terrain with neutral stratification) where the DA was made from 8 masts distributed across the domain. Validation of this approach was made with the Høvsøre case by contrasting the obtained results with data from measurements campaigns and literature. The obtained results shows that it is possible to obtain more accurate predictions that replicate the turbulent wind behavior at simulated scales and that, in addition, data assimilation improves the flat terrain prediction by 10%. In complex terrain, the data assimilation fails to improve the solution due to the proximity of the measurements with the ground and the terrain induced forcing.

Keywords: Multiscale Simulation, LES, Data Assimilation, High Resolution, Complex Terrain, WRF, Planetary Boundary Layer, Wind Resource Assessment.

Received xx de xx de 2019

Accepted xx de xx de 2019

1 Introduction

Having a precise prediction for the wind velocity in very localized zones has become a relevant necessity for some productive activities like: wind resource assessment, dispersion control of gases and toxic particulate material and also natural disasters like wildfires and tornadoes.

Historically two ways has been taken to predict wind behavior. The first is an statistical approach that uses data from several meteorological masts or other instrumentation located in a domain to extrapolate information to a time of interest. This approach present some weakness: (i) dependency of the instrumentation, (ii) the historical databases can't capture actual and local conditions of the atmosphere such as climate change, and (iii) the statistical values don't show the behavior of the continuous terrain but in some arbitrary points. Is because this that for more specific goals a second approach is used: the Numerical Weather Prediction (NWP). The NWP target is to find the future state of the meteorological variables integrating the system of partial differential equations that models the atmosphere behavior. One of the most relevant property of this system is the presence of multiples scales, i.e. the preponderant forces that governs the air dynamics vary depending of the space-temporal scale to analyze. Is convenient then to separate the spatial dependence associating a characteristic length to the domain of interest, in this way a global scale, synoptic scale, mesoscale and microscale can be defined.

The scales multiplicity introduces a new challenge to overcome: the computational cost of solving a system of equations valid for the entire atmosphere. As a consequence of this, a spectrum of numerical models have been created specifically for each spatial scale with their own equations, but the initialization of a small-scale model requires the results of a larger one.

With respect to global models, these have shown to be able to correctly simulate many aspects of the general circulation of the atmosphere ([Stocker et al. 2013](#)), however, for engineering interests, the focus is on the local behavior of the wind, specifically, how it moves within the planetary boundary layer (PBL) which is the part of the atmosphere we inhabit and that is outside the resolution of global models.

The approach being used today for small-scale atmospheric simulation, i.e. solving the structures belonging to the PBL, is through the so-called dynamic downscaling, interpolating the results from a large-scale model to a small-scale model in order to function as a boundary condition and generate a forecast in a finer mesh. This method defines what is understood by multi-scale simulation and this type of simulation is still widely discussed by the scientific community ([Arnold et al. 2010](#)).

The use of dynamic downscaling proved to be successful at least in the spectrum of global and synoptic scales. Numerical issues arise in the mesoscale due to terrain forcing and the relevance of local surface fluxes. The reduction to the microscale causes the increase in the relevance of turbulent stresses in the equations, requiring a much more precise handling.

Due to the space-time numerical grid dimensions in large scale models, the turbulence associated with the interaction with the surface and the thermal effects are generally parameterized through a turbulent viscosity. In scales close to the microscale, the models start natively to solve the turbulent structures generating a problem due to the double weighting of these structures as they are being solved on the one hand and parameterized on the other. This zone is known as the grey zone ([Wyngaard 2004](#)) and an incorrect configuration of the dynamic downscaling in this zone can cause non-physical results of the model. At the microscale it is possible to represent the turbulence according to known numerical models such as LES or RANS depending on the case. Atmospheric models such as WRF have been widely used in recent years to predict wind behavior at the mesoscale through multiscale simulations, but only a few studies have addressed this behavior at the microscale in real simulations. The researches that analyze the behavior of the LES to represent the PBL generally use ideal conditions (e.g. periodic boundary conditions, flat terrain, imposed pressure gradients) which allows the validation of the approach, but at the cost of losing the operativeness of working in a realistic scenario. Simulating a real case implies the use of high resolution databases for terrain elevation and land use category. In this work, in order to obtain the best possible solution for a short-term wind forecast in PBL, the use of a 4D data assimilation system was also considered with measurements obtained in the surface proximity within the simulation time window.

Lastly, the philosophy of this work is to establish the foundations of a new method for assessing the wind resource without relying on ad hoc idealizations, but through fundamental physics and the correct implementation of state-of-the-art instrumentation. The results obtained will serve as a benchmark for future verification of new or experimental models that perform high-resolution simulations in real terrain.

The article is structured as follows. First, the methodology is presented, detailing the numerical model, the parameterization of the turbulence, the process of data assimilation and the experimental designs. Then, the first and second order results obtained are shown together with the corresponding analyses for the cases without and with data assimilation. Finally, the conclusions and benefits of this system are presented and general guidelines are given for future work, such as its application in complex geometry.

2 Numerical Model

2.1 WRF Atmospheric Model

WRF is a state-of-the-art numerical mesoscale model that represent the latest scientific and engineering developments in climate prediction. It is open source, flexible, portable and efficient so that it allows simulations on both notebooks and massively parallelized supercomputers ([Skamarock et al. 2008](#)).

This model solves the non-hydrostatic Euler equations for fully compressible flow through a finite difference

scheme. Spatial discretization is carried out through a C-Arakawa horizontal grid and a ground-following vertical grid based on hydrostatic dry air pressure. The temporal integration is carried out with a 2nd order Runge-Kutta scheme.

The pressure waves that appear due to the model compressibility are filtered from the mean field through a divergence filter and are resolved in a time sub-step (1/3 of the external mode) ensuring the stability of the scheme.

The boundary conditions are specified from the results of a global model for the horizontal boundaries. A constant pressure condition with a damping layer at the upper boundary and wall functions are used at the soil surface through the surface layer parametrization. The initial condition also comes from a global model results. The high resolution is achieved by combining the dynamic downscaling of nested domains with the implementation of new databases for static information. The initialization of the internal domains is done through the downscaling of the results of the parent domains. In this way we will talk about mesoscale domains for those that meet $\Delta x > 1000$ (m) and microscale for $\Delta x < 500$ (m).

The physical phenomena that are outside the model's mesh resolution are parameterized through several advanced schemes provided by WRF. Radiation, phase-change, cloud formation, surface interaction, boundary layer transport and turbulence are all considered within the model and are included in the right side of the equations as dependent terms.

Regarding turbulence, for the mesoscale it is represented by a vertical eddy viscosity that is computed in the PBL parametrization subroutine, while the horizontal eddy viscosity is computed through a Smagorinsky closure ([Smagorinsky 1963](#)). On the microscale, the PBL parametrization is turned off and a LES 1.5TKE model is used ([Deardorff 1980](#)).

2.2 Large Eddy Simulation and Sub-Grid Stress

The application of a Large Eddy Simulation (LES) model for the turbulence in the micro-scale implies the use of a low-pass filter on the independent variables as:

$$\tilde{\varphi}(x_j, t) = \int G(r_i, x_j) \varphi(x_j - r_i, t) dr_i, \quad (1)$$

where φ represents any variable. The kernel G allows the filtering of every variation whose scale is smaller than the filter width Δx . For the WRF software, the filtering operation is a numerical consequence of the spatial mesh and therefore is called an implicit filter. In the micro-scale all the variables of the model represent filtered variables.

The result of applying the filtering operation to the momentum equation is the creation of a non-closed term for the sub-grid stress τ_{ij} of the form,

$$\tau_{ij} = \widetilde{u_i u_j} - \widetilde{u}_i \widetilde{u}_j, \quad (2)$$

\widetilde{u}_i corresponds to the filtered/resolved velocity components in the (x, y, z) directions. The closure of τ_{ij} requires the implementation of a new equation that relates the stresses to known variables. For this paper, closure is accomplished using the 1.5TKE model which expresses the anisotropic sub-grid stresses τ_{ij}^r as a function of a turbulent viscosity ν_t and the resolved strain rate \widetilde{S}_{ij} in the form,

$$\tau_{ij}^r = \tau_{ij} - \frac{1}{3} \tau_{nn} \delta_{ij} = -2\nu_t \widetilde{S}_{ij}. \quad (3)$$

Here δ_{ij} is the Kronecker delta and the \widetilde{S}_{ij} tensor is defined as

$$\widetilde{S}_{ij} = \frac{1}{2} \left(\frac{\partial \widetilde{u}_i}{\partial x_j} + \frac{\partial \widetilde{u}_j}{\partial x_i} \right). \quad (4)$$

The LES package in WRF ([Yamaguchi and Feingold 2012](#)), expresses the turbulent viscosity as

$$\nu_t = c_k \ell \sqrt{k}, \quad (5)$$

where c_k is the constant of the model ($0.15 \sim 0.30$) and k is the sub-grid kinetic energy defined as:

$$k = \frac{1}{2}\tau_{nn}. \quad (6)$$

The characteristic length ℓ of the model is calculated as:

$$\ell = \begin{cases} \min[(\Delta x \Delta y \Delta z)^{1/3}, 0.76\sqrt{k}/N] & N^2 > 0 \\ (\Delta x \Delta y \Delta z)^{1/3} & N^2 \leq 0 \end{cases} \quad (7)$$

N is the Brunt-Väisälä frequency for humid air.

Finally, the value of k in each domain cell is calculated based on the transport equation defined by [Skamarock et al. \(2008\)](#).

2.3 Data Assimilation Process

From the WRF model, three-dimensional arrays of the resolved meteorological variables are obtained for a given time (background). The data assimilation goal is to physically weight the field measurements (observations) with these results to obtain the best estimate of the state of the atmosphere (analysis).

Theoretically, the data assimilation process tries to minimize the cost function $J(x)$ that weighs the errors coming from the background J_b and from observations J_o :

$$J(x) = J_b + J_o \quad (8)$$

$$J(x) = \frac{1}{2}(x - x_b)^T B^{-1}(x - x_b) + \frac{1}{2}(Hx - y)^T R^{-1}(Hx - y) \quad (9)$$

Here B is the background variance or error matrix and R is the observation error matrix.

The observation operator H performs a 3D interpolation of the numerical grid values to the observation space. The variational problem is solved for the value $x = x_a$ which nullifies the cost function gradient:

$$\nabla J(x) = B^{-1}(x - x_b) - H^T R^{-1}(Hx - y) = 0 \quad (10)$$

The increment can then be expressed as:

$$x_a - x_b = BH^T(HBH^T + R)^{-1}(y - Hx_b) \quad (11)$$

The above equation can be interpreted by recognizing that $H B H^T$ is the background error projection in the observation space and $B H^T$ is another projection but in the background-observation space. The result is therefore a weighted projection of the gap between the observations and the background.

In WRF the solution is calculated with the following variable changes in mind:

$$y'_o = y_o - Hx_b \quad (12)$$

$$x' = Uv = x - x_b \quad (13)$$

Where U is defined such that:

$$UU^T \approx B \quad (14)$$

v is a so-called control variable. Note that y'_o is the innovation vector, that is, the difference between the observation and the background. x' is the analysis increment.

Under these new variables the variational problem is written as:

$$J(v) = \frac{1}{2}v^T v + \frac{1}{2}(y'_o - \bar{H}Uv)^T R^{-1}(y'_o - \bar{H}Uv) \quad (15)$$

\bar{H} is the linearized observation operator.

In practice, U is a recursive application of several filters that allow the assimilation process to be less costly and that the control variable complies the atmospheric balances. The equation is solved recursively for v using a Quasi-Newtonian minimization algorithm.

3 Case Study Settings

The goal of this study is to evaluate the behavior of the WRF mesoscale model in its LES mode when forced up to 3m mesh size and incorporating surface data assimilation to solve the structures developed within the PBL. Five experiments were developed for this purpose. The first two were carried out at Høvsøre for the case without (H2) and with (H2) data assimilation. The last three correspond to simulations made in the Bolund Hill for the case without (B1) and with (B2-B3) data assimilation. Case B3 corresponds to a simulation with data assimilation extrapolated surface values.

3.1 Høvsøre Setup (H1 and H2)

Høvsøre is a wind turbine test site located in Denmark. Historically, many studies have been conducted at this site because of its relatively homogeneous and flat surface ([Peña et al. 2015; 2013](#)), and therefore it is useful to validate numerical results of experimental models. The site counts with a meteorological mast, whose data are public, facilitating the access to the measurements for the data assimilation process ([Floors et al. 2013](#)). The simulation performed consists of a total of 14 hours, where the first 6 correspond to the spinup of the model and the time window where the data assimilation is applied. The date of the simulation were selected in such a way that it corresponds to a period with neutral atmospheric stability as declared by [Peña et al. \(2013\)](#) in its case 5. Table 1 shows the main aspects of the H1 and H2 experiments.

Table 1: Numerical domain for H1 and H2 experiments.

Parameter	Selection
Date	2010-09-08 06:00:00 to 20:00:00 UTC
Top BC	30000 [Pa]
# Domains	7
Domain Centre	(56.440588, 8.150896)

The initial condition and the boundary condition for the coarser mesh is given by the operational analysis of the GFS global model with 0.5° of resolution. The boundary condition is mapped to the first domain contours using a buffer zone of 5 elements of mesh and are updated every 6 hours.

The extension configuration of the domains was subjected to a sensitivity analysis in order to adjust the best values in order to ensure: (i) the model stability, (ii) the convergence of results for the boundary layer and (iii) the lowest computation time. In this fashion, the number of elements for the mesh and the top boundary condition are established. The number of nodes in all the domains are set as $107 \times 107 \times 37$.

For the downscaling, 7 nested domains with feedback were used, all of which were centered on the meteorological mast location. The subdomains were selected to avoid the double weighting due to the turbulent grey zone using a ratio of 5 for the telescopic generation of the d4 and d5 domains, where the shift to the microscale occurs (a technique validated by [Green and Zhang \(2015\)](#)). A spatial reference of the nested domain distribution can be seen in Figure 1.

The simulation's high resolution is achieved through the implementation of non-native WRF databases. The ASTER database is used for the terrain height. For land use, the Corine 2012 database transformed to its

Table 2: Characteristic values and databases of each domain for H1 and H2.

Domain	d1	d2	d3	d4	d5	d6	d7
$\Delta x = \Delta y$ [m]	30000	10000	3333.3	1111.1	222.22	74.074	24.691
Δt [s]	75	25	8.333	2.778	0.556	0.185	0.062
Terrain DB	GMTED	GMTED	GMTED	ASTER	ASTER	ASTER	ASTER
LU DB	USGS	USGS	USGS	CLC12	CLC12	CLC12	CLC12

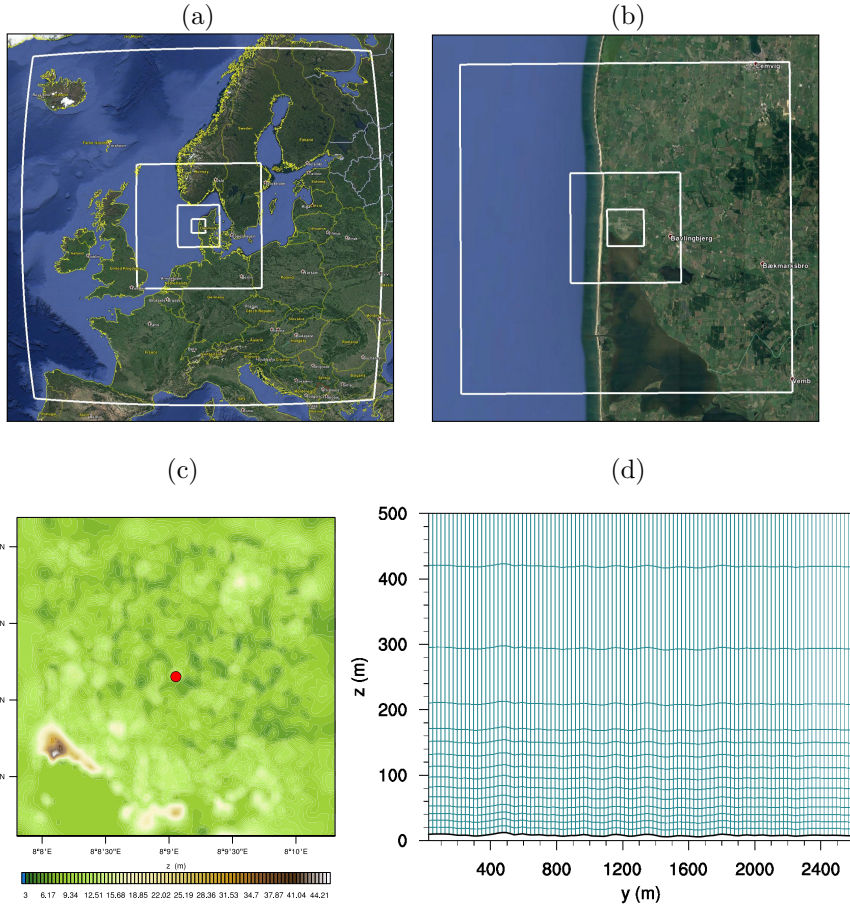


Figure 1: Simulation domains for H1 and H2. (a) Domains d1-d4. (b) d5-d7. (c) Detail of d7 with the control point. (d) Vertical grid distribution on a 4:1 scale.

analogue USGS24 is used for the interpretation of the code ([Pineda et al. 2004](#)). A value of $z_0 = 1.5$ [cm] is manually assigned for the surface of the innermost domain ([Peña et al. 2013](#)). The Table 2 shows the differences of each subdomain.

For the vertical mesh, special care is taken to refine it so it is consistent with the application of the LES. In the first level there is an aspect ratio of $\Delta_x/\Delta_{z_1} = 2.35$ and this is progressively reduced in the higher levels. Figure 1(d) shows the mesh detail for the first 500m in the vertical.

The selection of the settings was made in agreement with other similar works in the literature and can be seen in Table 3.

Finally, the public data from the meteorological mast were used to feed the data assimilation process. The frequency at which the background is corrected is set at 10 minutes and is performed during the first 6 hours of the simulation. The variables that were assimilated are wind speed and direction, and are assimilated at 5 heights: 10, 40, 60, 80 and 100 meters above the ground.

3.2 Bolund Setup (B1, B2 and B3)

Bolund is a 12 [m] high, 130 [m] long and 75 [m] wide seaside hill located in Denmark. Thanks to the measurement campaign made by [Bechmann et al. \(2009\)](#) and its posterior blind model comparison ([Berg et al. 2011; Bechmann et al. 2011](#)), this is an optimal location for the testing of experimental computational models in the context of complex terrain. The measurement campaign provides Bolund with information on 10 masts distributed across and close to the hill, as well as high resolution data for terrain height and roughness length. The conducted experiments consisted of 9 hours of simulation, with the first 6 hours being the spinup of the model. The date was selected according to what was declared by [Bechmann et al. \(2009\)](#) for a day with the

Table 3: Model physics for H1 and H2.

Domain	d01	d02	d03	d04	d05	d06	d07
Micro-physics	WSM5						
Cumulus	Grell	Grell	—	—	—	—	—
Superficial Layer	MYNN						
PBL	MYNN	MYNN	MYNN	MYNN	—	—	—
LES model	—	—	—	—	1.5TKE	1.5TKE	1.5TKE
c_k	—	—	—	—	0.3	0.3	0.3
Soil model	Difus.						
LWR	RRTM						
SWR	Dudhia						

most neutral stratification possible. More information is presented in the Table 4.

Table 4: Numerical domain for B1, B2 and B3 experiments.

Parameter	Selection
Date	29-12-2007 06:00 to 15:00 UTC
N_z	41
Top BC	30000 [Pa]
# Domains	8
Domain Centre	(55.703474, 12.098854)
Nodes	3.465.000

De la misma forma que para el caso de Høvsøre, las condiciones iniciales y de borde provenienan del modelo GFS. Debido a las dimensiones de la colina, se utilizaron 8 dominios anidados para el escalamiento dinámico como se puede ver en la Figura 2. Todos los dominios constan de 107×107 nodos en la horizontal, exceptuando el dominio mas interior d8 que es de 107×92 debido a la extensión de la base de datos entregada por la campaña de medición. Para el manejo de la zona gris se utiliza el mismo acercamiento que para los experimentos H1 y H2.

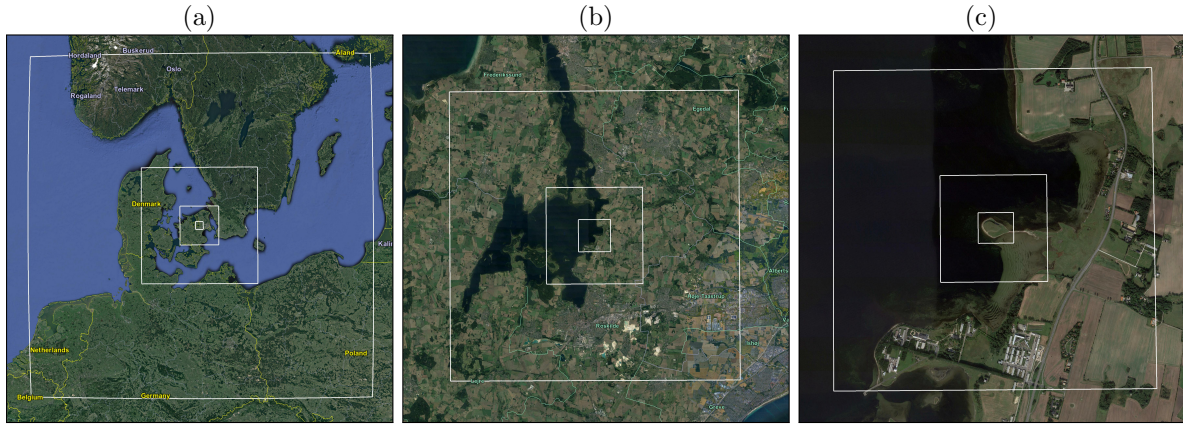


Figure 2: Simulation domains for B1, B2 and B3. (a) d1-d4. (b) d4-d6. (c) d6-d8.

Con respecto a la alta resolución, se vuelven a utilizar las bases de datos CLC12 y ASTER para los dominios intermedios. Para el dominio d8 se incorporaron a WRF las bases de datos de uso de suelo y altura del terreno entregadas por los desarrolladores de la campaña de medición. Estas bases de datos poseen una resolución de

25 [cm], lo cual es suficiente para la malla mas interior con resolución de 3 [m]. El largo de rugosidad se fija en $z_0 = 1.5$ [cm] (Bechmann et al. 2011).

Debido a la pendiente abrupta de la colina, un refinamiento de la malla vertical fue realizado para evitar inestabilidades. De esta manera se fija la cantidad de nodos en la vertical como $N_z = 41$

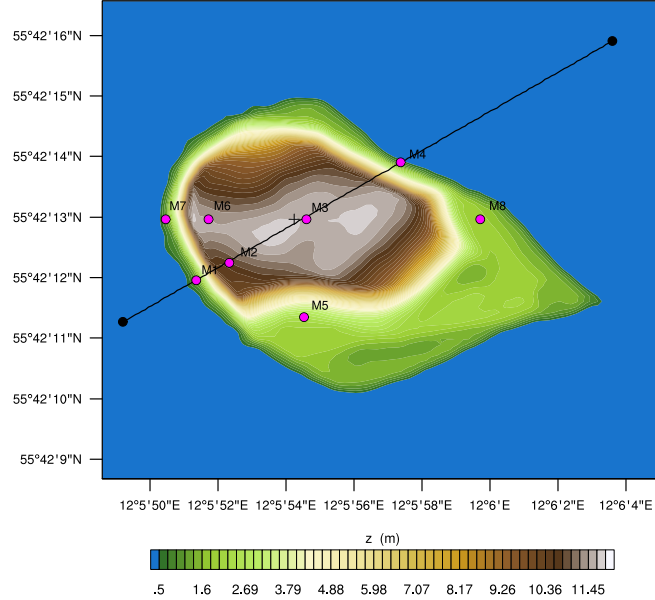


Figure 3: Control points locations for B1, B2 and B3.

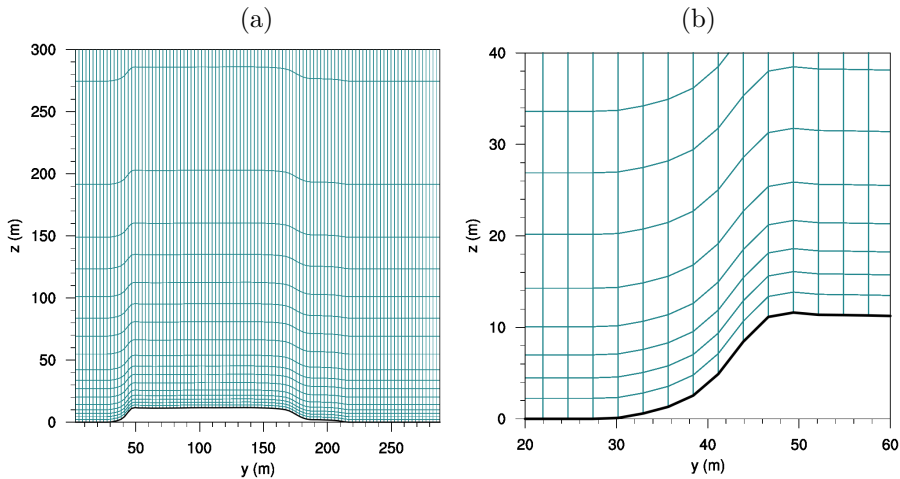


Figure 4: (a) Vertical mesh distribution in the middle of d8. (b) Detail of the steep slope on a 1:1 scale.

Table 5: Characteristic values of each domain for B1, B2 and B3.

Dominio	d1	d2	d3	d4	d5	d6	d7	d8
Δx [m]	10000	3333.3	1111.1	222.22	74.074	24.691	8.23045	2.74348
Δt [s]	12	4	1.3333	0.4444	0.0889	0.0296	0.0099	0.0033
Terrain DB	GMTED	GMTED	GMTED	ASTER	ASTER	ASTER	ASTER	Bolund
LU DB	USGS	USGS	USGS	CLC12	CLC12	CLC12	CLC12	Bolund

Table 6: Model Physics for B1, B2 and B3

Domain	d1	d2	d3	d4	d5	d6	d7	d8
Micro-physics	WSM5							
Cumulus	Grell	–	–	–	–	–	–	–
Superficial Layer	MYNN							
PBL	MYNN	MYNN	MYNN	–	–	–	–	–
LES model	–	–	–	1.5TKE	1.5TKE	1.5TKE	1.5TKE	1.5TKE
c_k	–	–	–	0.2	0.2	0.2	0.2	0.2
Soil model	Difus.							
LWR	RRTM							
SWR	Dudhia							

3.3 Error Estimation

To evaluate the performance of the simulations in relation to the real data, the RMSE and the MAE are used as metrics.

$$MAE = \frac{1}{n} \sum_{i=1}^n |y_i - x_i| \quad (16)$$

$$RMSE = \sqrt{\frac{1}{n} \sum_{i=1}^n (y_i - x_i)^2} \quad (17)$$

The evaluation of the metrics is performed after the spinup time and each of the measured values is compared with the nearest simulated value, interpolated to the corresponding height in the mast. The interpolation is made using a simple logarithmic law for the wind profile,

$$u(z) = u(z_r) \frac{\ln(z/z_0)}{\ln(z_r/z_0)} \quad (18)$$

Where z_0 is the corresponding roughness length for each case.

Finally, Pearson's coefficient will also be used as an indicator of proportionality between the simulated and measured data.

$$r = \frac{\sum_{i=1}^n [(x_i - \bar{x})(y_i - \bar{y})]}{\left[\sum_{i=1}^n (x_i - \bar{x})^2 \right]^{1/2} \left[\sum_{i=1}^n (y_i - \bar{y})^2 \right]^{1/2}} \quad (19)$$

4 Results

4.1 Høvsøre

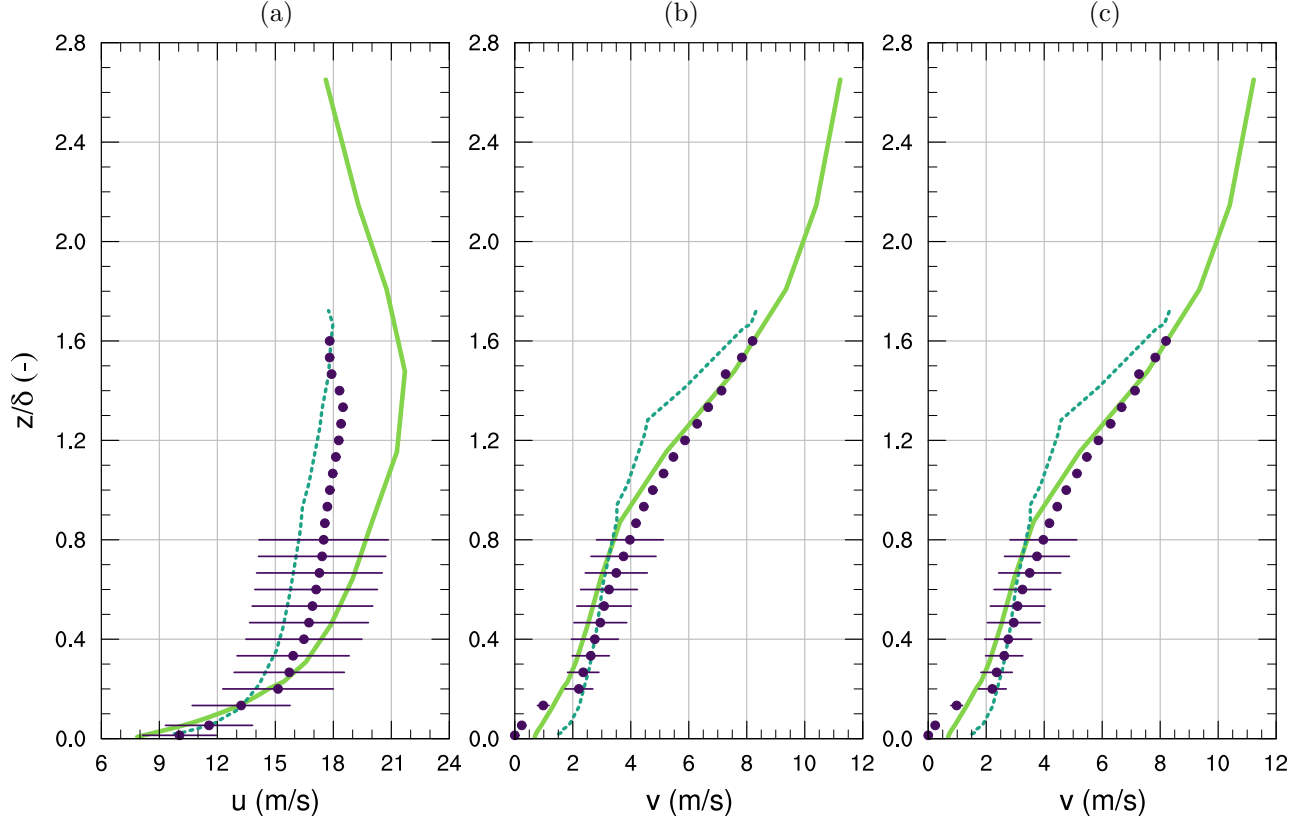


Figure 5: Comparación de la simulación (línea continua) con la simulación de Peña et. al. en el 2013 (línea punteada) y valores medidos para (a) componente u de la velocidad del viento, (b) componente v y (c) magnitud de la velocidad del viento. Los datos corresponden a promedios temporales entre las 12:00 y 15:00, y han sido rotados de tal forma que su dirección sea 0° a los 10m.

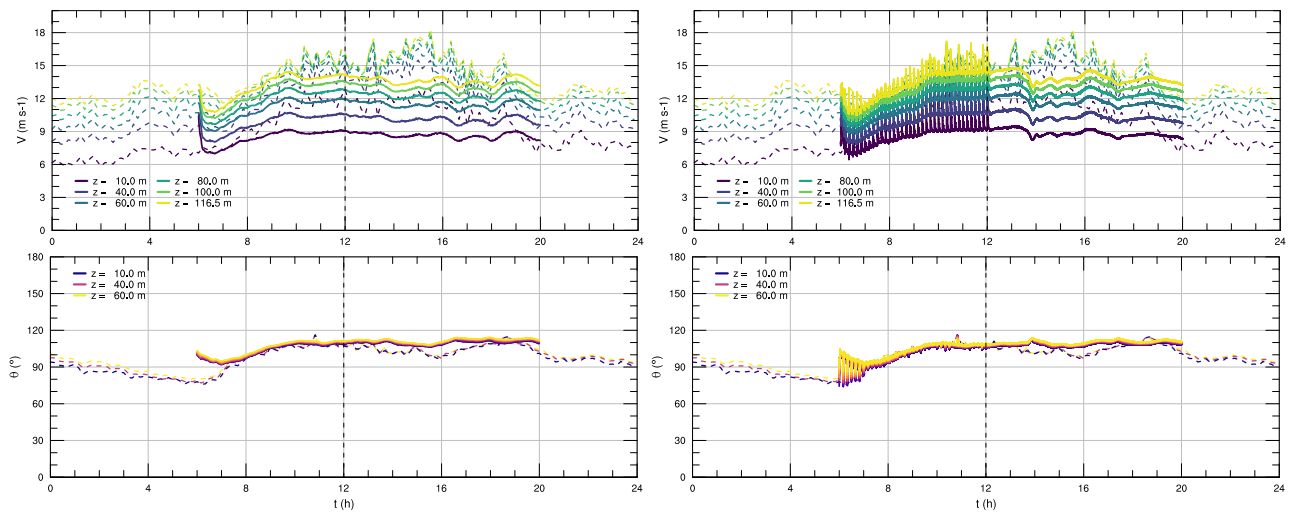


Figure 6: aaaaa

5 Acknowledgements

Los autores de este artículo quieren agradecer a fondef, dgip, hovsore

Figuras (temporal)

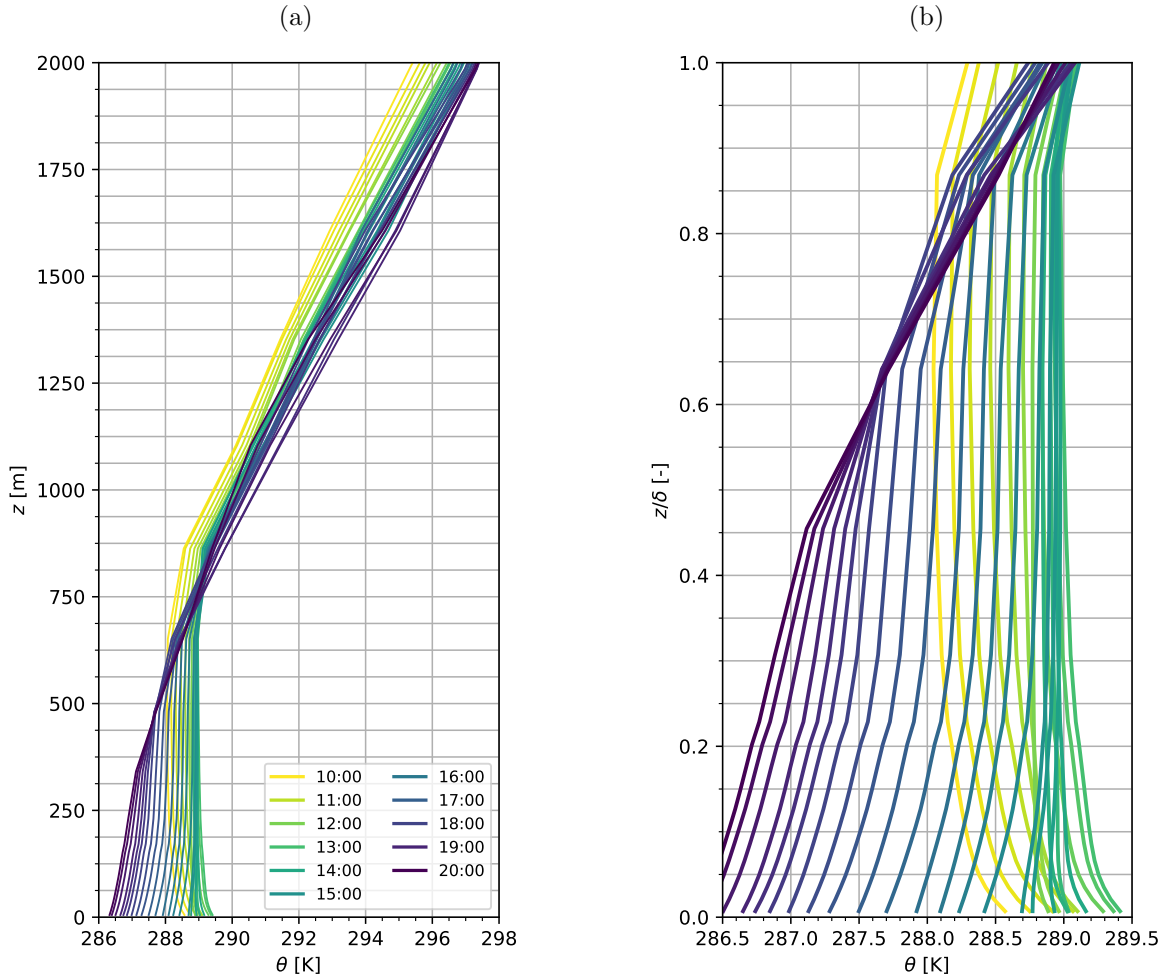


Figure 7: Ciclo diurno-nocturno del perfil de temperatura potencial en el mástil meteorológico. (a) Resultados cada 20 minutos del perfil de θ_v . (b) Corresponde al detalle del perfil dentro de la capa límite atmosférica ($\delta \approx 750$ [m]).

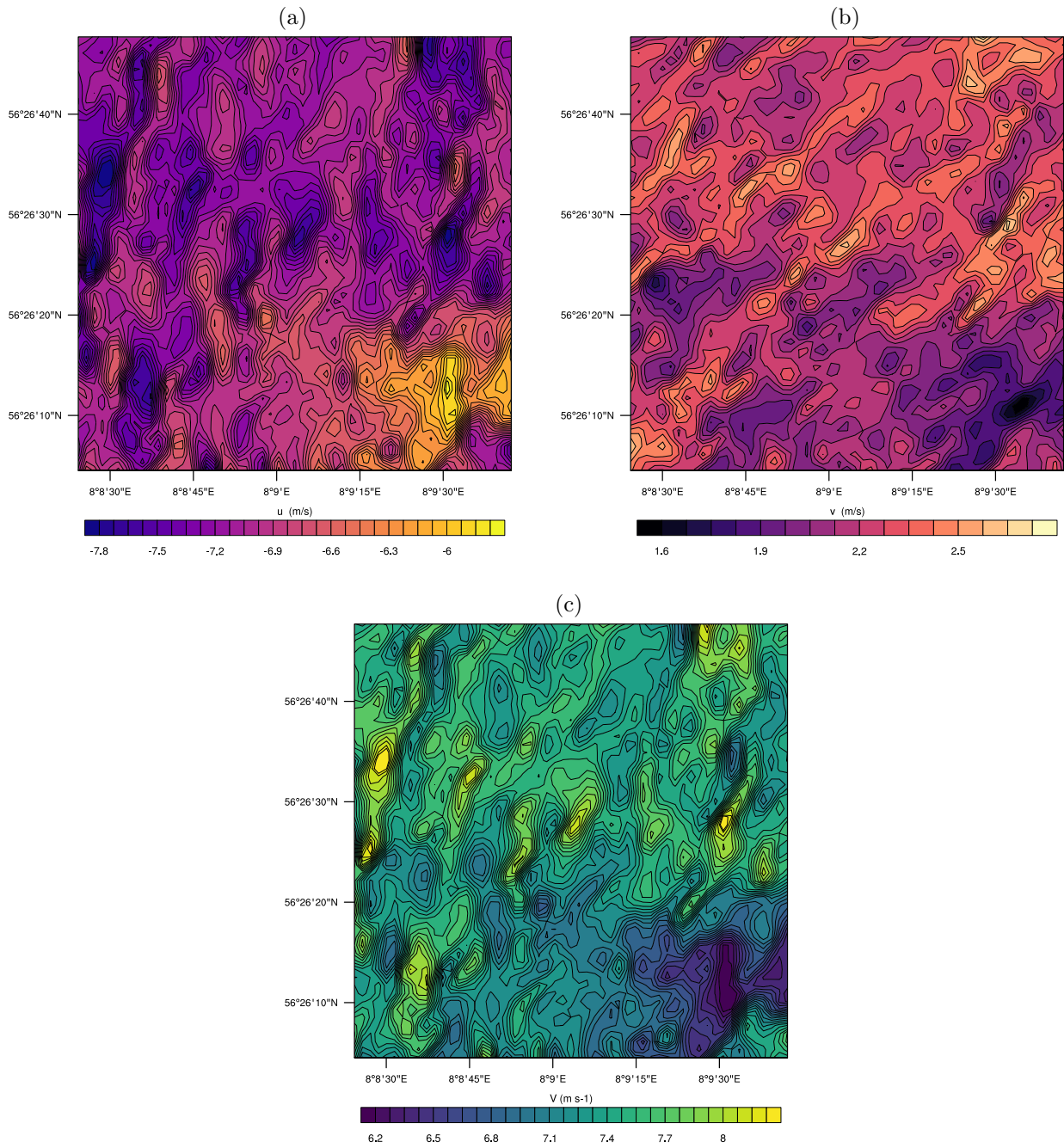


Figure 8: (a) Componente u de la velocidad en el primer nivel de la coordenada vertical ($z_1 = 5.25$ [m]) para las 15:00. (b) Idéntico al anterior pero para la componente v . (c) Magnitud del campo de velocidad.

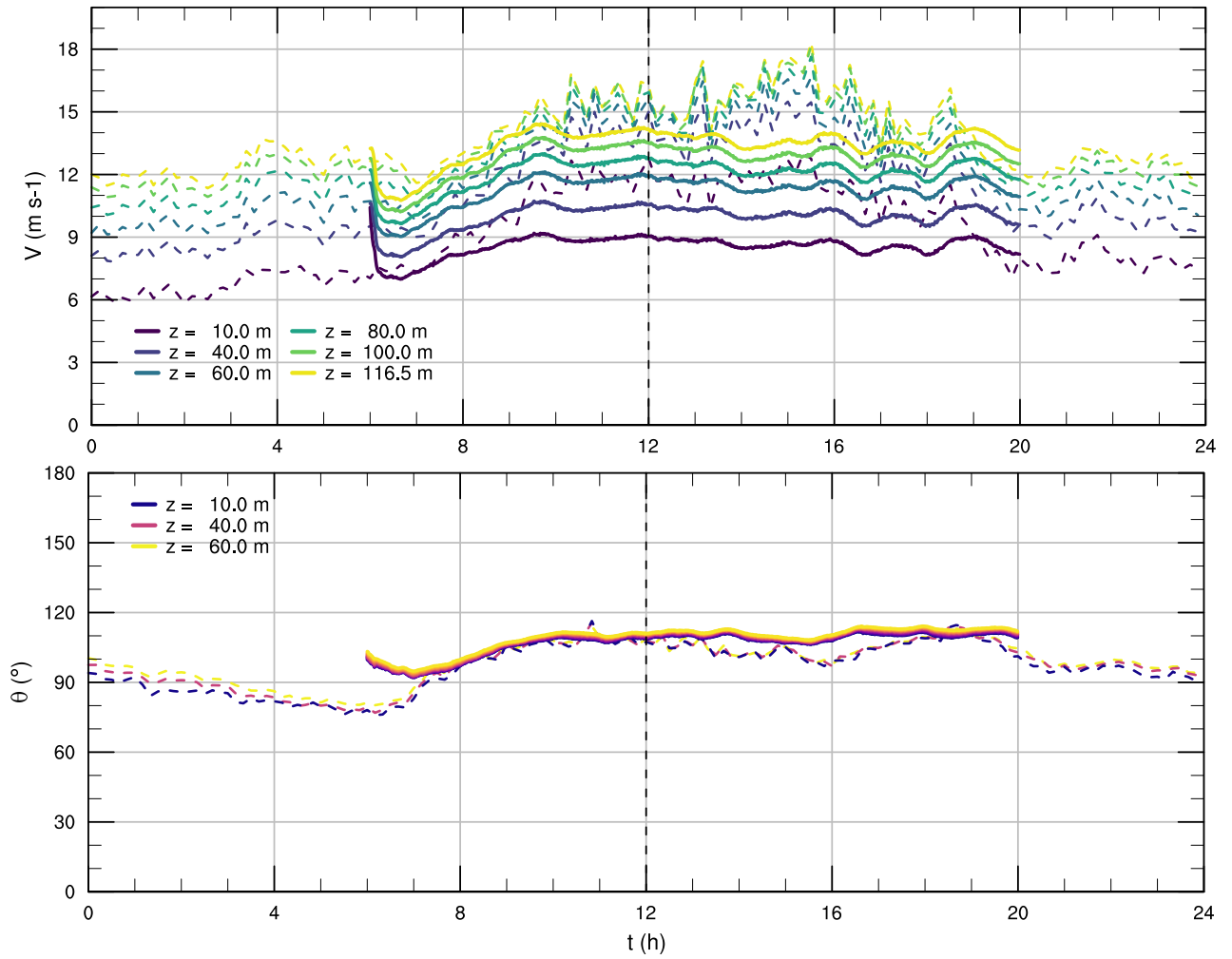


Figure 9: Serie de tiempo para la rapidez instantánea del viento V y su dirección en la ubicación del mástil meteorológico. La línea continua corresponde a los datos simulados interpolados a las alturas de medición (solo para V) y la línea punteada a los datos medidas en el mástil.

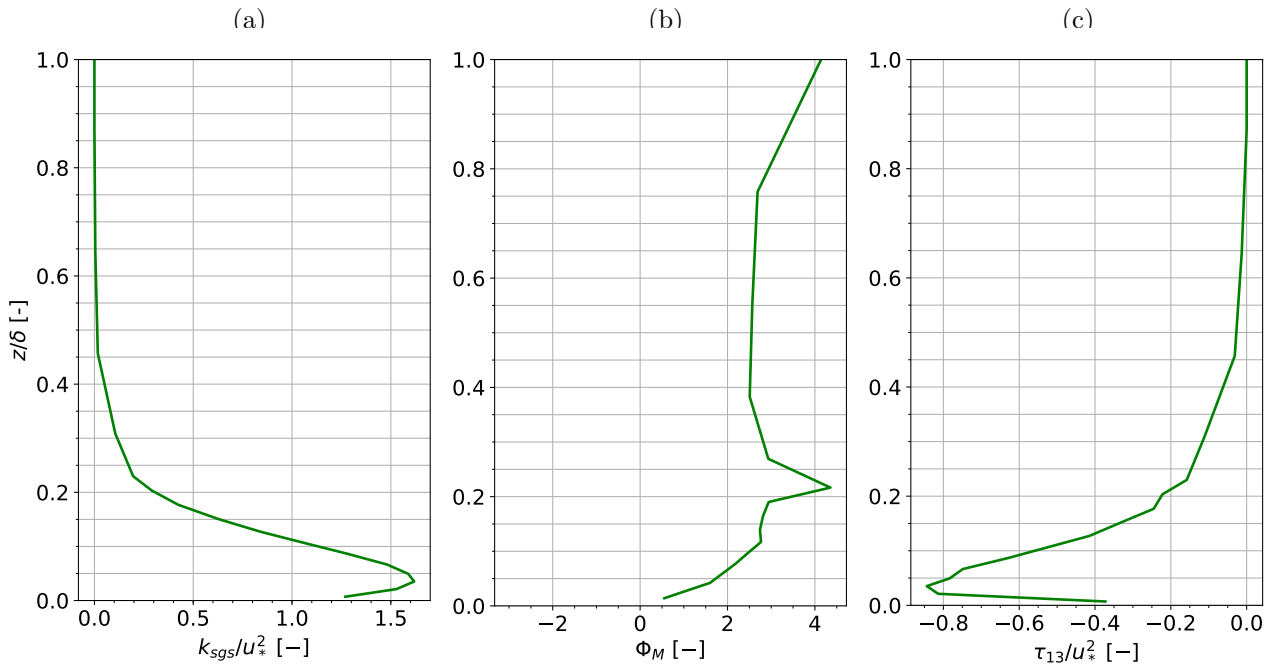


Figure 10: Variables adimensionadas ($u_* = 0.552$ [m/s]) de segundo orden para el caso de Høvsøre promediados entre las 12:00 y las 15:00 (atmósfera neutra, terreno plano homogéneo). (a) Energía cinética turbulenta de submallada, (b) Gradiente de velocidad, (c) Esfuerzo turbulento.

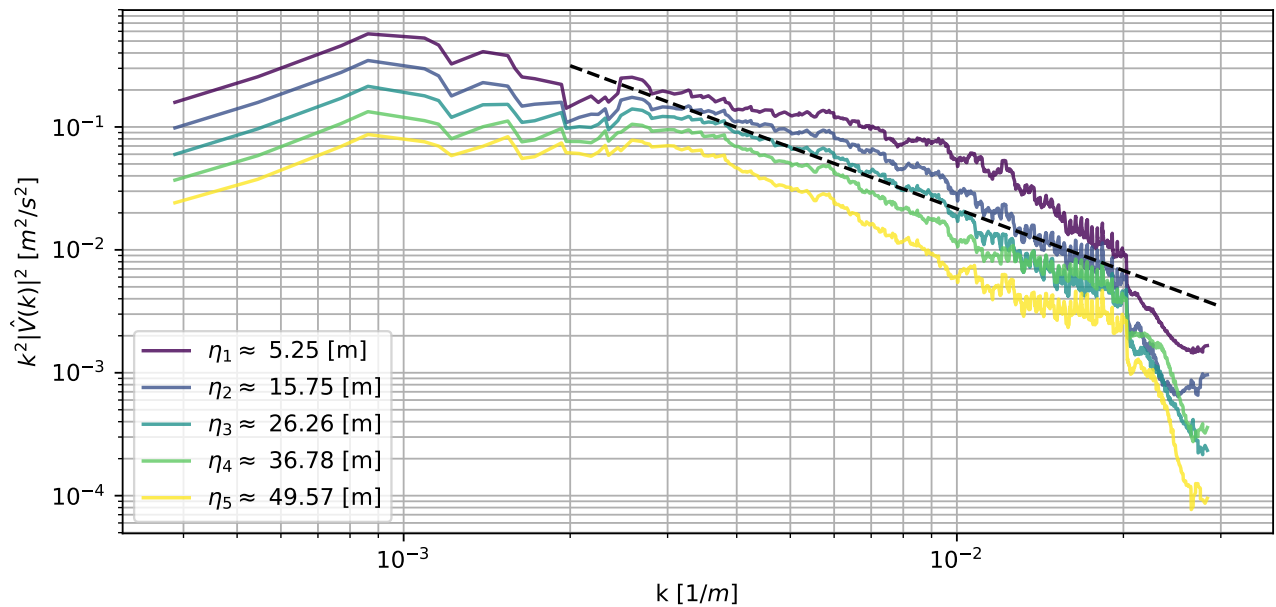


Figure 11: Espectros de energía para la componente horizontal del viento a distintos niveles verticales en el dominio d07 caso Høvsøre.

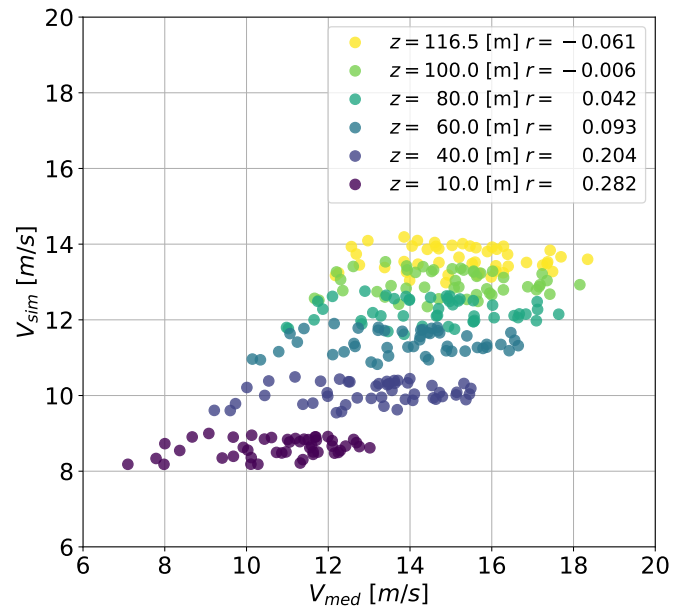


Figure 12: Gráfico de dispersión para las velocidades a distintas alturas en el mástil meteorológico de Høvsøre.

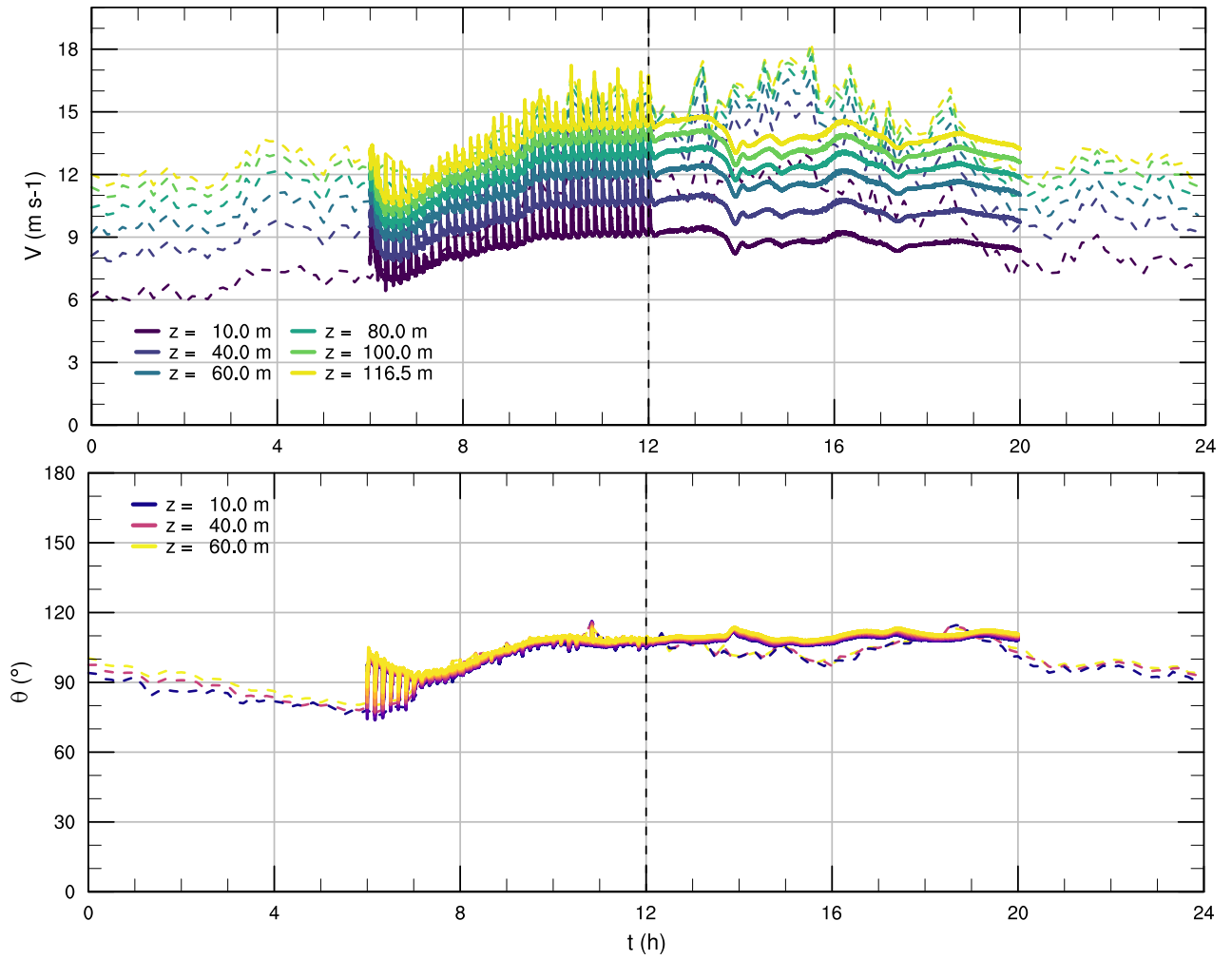


Figure 13: Serie de tiempo para la rapidez instantánea del viento V y su dirección en la ubicación del mástil meteorológico para el caso con asimilación de datos. La línea continua corresponde a los datos simulados interpolados a las alturas de medición (solo para V) y la línea punteada a los datos medidas en el mástil.

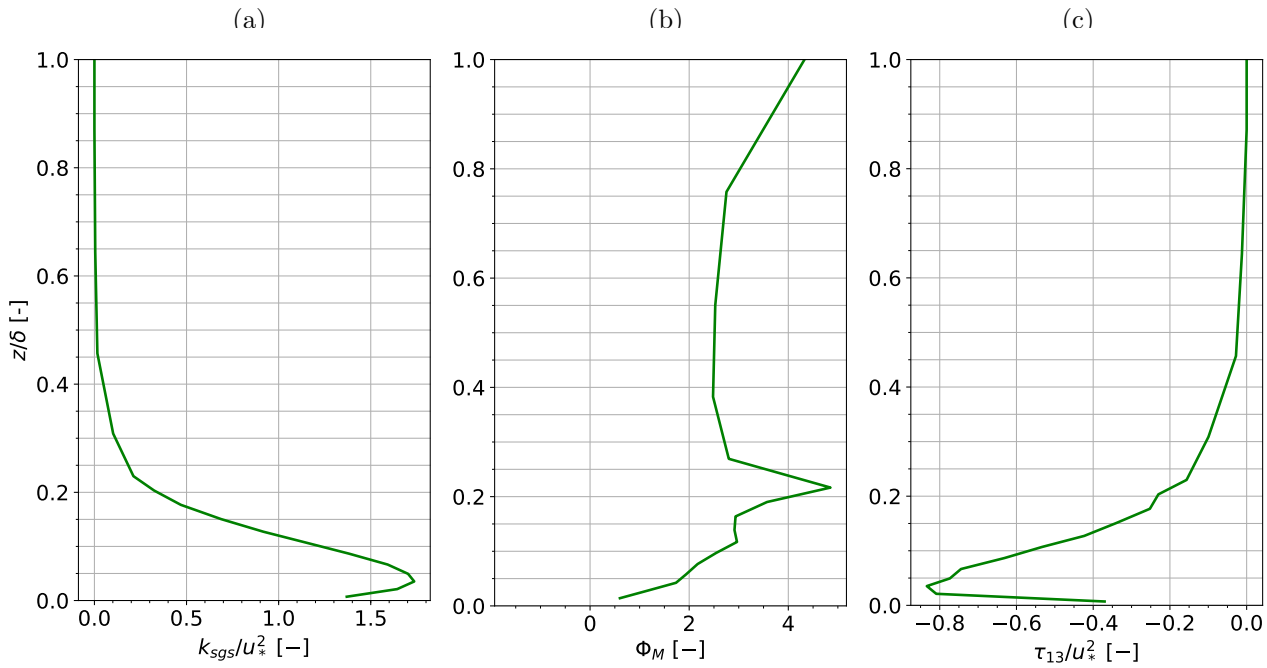


Figure 14: Variables adimensionadas ($u_* = 0.527$ [m/s]) de segundo orden para el caso de Høvsøre con DA promediados entre las 12:00 y las 15:00 (atmósfera neutra, terreno plano homogéneo). (a) Energía cinética turbulenta de submalla, (b) Gradiente de velocidad, (c) Esfuerzo turbulento.

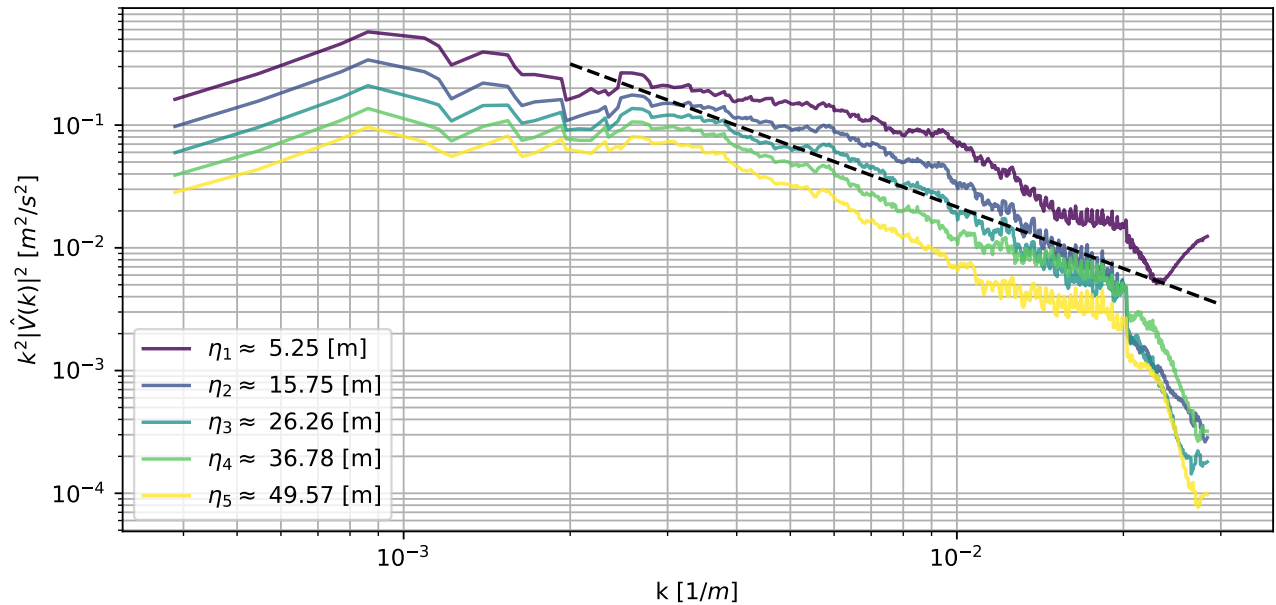


Figure 15: Espectros de energía para la componente horizontal del viento a distintos niveles verticales en el dominio d07 caso Høvsøre con DA.

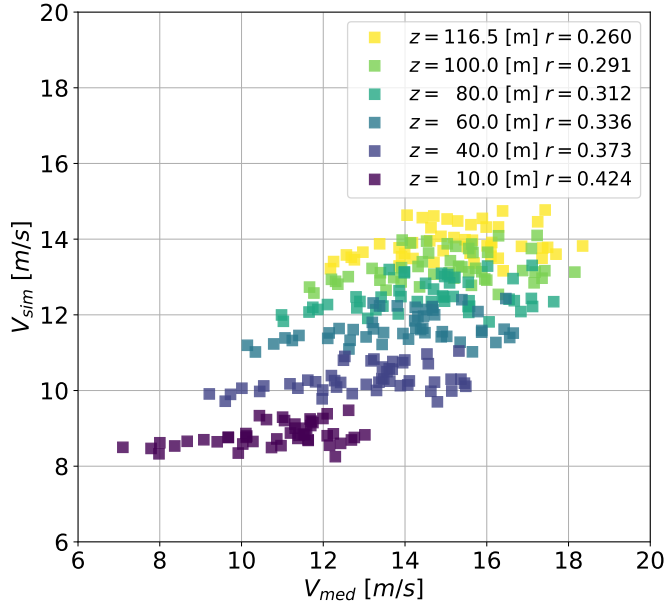


Figure 16: Gráfico de dispersión para las velocidades a distintas alturas en el mástil meteorológico de Høvsøre (con DA).

Table 7: Comparación de métricas para el caso I Høvsøre.

	Sin DA	Con DA
MAE	2.41091 m/s	2.16742 m/s
RMSE	2.80142 m/s	2.55778 m/s
ΔRMSE	–	8.70%
ΔMAE	–	10.47%

References

- Arasa R, Porras I, Domingo-Dalmau A, Picanyol M, Codina B, González MÁ, Piñón J (2016) Defining a standard methodology to obtain optimum WRF configuration for operational forecast: Application over the port of Huelva (southern Spain). *Atmospheric and Climate Sciences* 06(02):329–350
- Arnold D, Schicker I, Seibert P (2010) High-resolution atmospheric modelling in complex terrain for future climate simulations (HiRmod). Tech. rep., Institute of Meteorology (BOKU-Met), University of Natural Resources and Life Sciences
- Arnold D, Morton D, Schicker I, Seibert P, Rotach M, Horvath K, Dudhia J, Satomura T, Müller M, Zängl G, et al. (2012) High resolution modelling in complex terrain: report on the HiRCOT 2012 Workshop, Vienna, 21–23 February 2012. Institut für Meteorologie, Department Wasser-Atmosphäre-Umwelt, Univ. f. Bodenkultur
- Barker D, Huang W, Guo YR, Bourgeois A (2003) A three-dimensional variational (3DVAR) data assimilation system for use with MM5
- Barker D, Huang XY, Liu Z, Auligné T, Zhang X, Rugg S, Ajjaji R, Bourgeois A, Bray J, Chen Y, Demirtas M, Guo YR, Henderson T, Huang W, Lin HC, Michalakes J, Rizvi S, Zhang X (2012) The weather research and forecasting model's community variational/ensemble data assimilation system: WRFDA. *Bulletin of the American Meteorological Society* 93(6):831–843

- Barker DM, Huang W, Guo YR, Bourgeois AJ, Xiao QN (2004) A three-dimensional variational data assimilation system for MM5: Implementation and initial results. *Monthly Weather Review* 132(4):897–914
- Bechmann A, Sørensen NN (2011) Hybrid RANS/LES applied to complex terrain. *Wind Energy* 14(2):225–237
- Bechmann A, Berg J, Courtney M, Ejsing Jørgensen H, Mann J, Sørensen N (2009) The Bolund Experiment: Overview and Background. Danmarks Tekniske Universitet, Risø Nationallaboratoriet for Bæredygtig Energi, risø-R-1658(EN)
- Bechmann A, Sørensen NN, Berg J, Mann J, Réthoré PE (2011) The bolund experiment, part II: Blind comparison of microscale flow models. *Boundary-Layer Meteorology* 141(2):245–271
- Berg J, Mann J, Bechmann A, Courtney MS, Jørgensen HE (2011) The bolund experiment, part I: Flow over a steep, three-dimensional hill. *Boundary-Layer Meteorology* 141(2):219–243
- Berselli L, Iliescu T, Layton WJ (2005) Mathematics of Large Eddy Simulation of Turbulent Flows (Scientific Computation). Springer
- Brasseur JG, Wei T (2010) Designing large-eddy simulation of the turbulent boundary layer to capture law-of-the-wall scaling. *Physics of Fluids* 22(2):021303
- Brown AR, Hobson J, Wood N (2001) Large-eddy simulation of neutral turbulent flow over rough sinusoidal ridges. *Boundary-Layer Meteorology* 98(3):411–441
- Burden R, Faires J (2010) Numerical Analysis. Cengage Learning
- Businger JA, Wyngaard JC, Izumi Y, Bradley EF (1971) Flux-profile relationships in the atmospheric surface layer. *Journal of the Atmospheric Sciences* 28(2):181–189
- Carati D, Winckelmans GS, Jeanmart H (2001) On the modelling of the subgrid-scale and filtered-scale stress tensors in large-eddy simulation. *Journal of Fluid Mechanics* 441
- Chaudhari A (2014) Large-eddy simulation of wind flows over complex terrains for wind energy applications. PhD thesis
- Cheng WY, Liu Y, Bourgeois AJ, Wu Y, Haupt SE (2017) Short-term wind forecast of a data assimilation/weather forecasting system with wind turbine anemometer measurement assimilation. *Renewable energy* 107:340–351
- Chow FK, Street RL (2009) Evaluation of turbulence closure models for large-eddy simulation over complex terrain: Flow over askervein hill. *Journal of Applied Meteorology and Climatology* 48(5):1050–1065
- Comisión Nacional de Energía de Chile (2018) Anuario Estadístico de Energía 2018
- Davidson P (2013) Turbulence in Rotating, Stratified and Electrically Conducting Fluids. Cambridge University Press
- Deardorff JW (1974) Three-dimensional numerical study of the height and mean structure of a heated planetary boundary layer. *Boundary-Layer Meteorology* 7(1):81–106
- Deardorff JW (1980) Stratocumulus-capped mixed layers derived from a three-dimensional model. *Boundary-Layer Meteorology* 18(4):495–527
- Doubrawa P, Montornès A, Barthelmie RJ, Pryor SC, Casso P (2018) Analysis of different gray zone treatments in WRF-LES real case simulations. *Wind Energy Science Discussions* 2018:1–23
- Dumais R, Kirby S, Flanigan R (2013) Implementation of the WRF Four-Dimensional Data Assimilation method of observation nudging for use as an ARL weather running estimate-nowcast. Tech. rep., ARMY RESEARCH LAB WHITE SANDS MISSILE RANGE NM COMPUTATIONAL AND INFORMATION

- Enriquez RM, Street RL (2017) An algebraic subgrid-scale model for large-eddy simulations of the atmospheric boundary layer. Tech. rep., Bob and Norma Street Environmental Fluid Mechanics Laboratory, Stanford University
- Floors R, Vincent CL, Gryning SE, Peña A, Batchvarova E (2013) The wind profile in the coastal boundary layer: Wind lidar measurements and numerical modelling. *Boundary-layer meteorology* 147(3):469–491
- Green BW, Zhang F (2015) Numerical simulations of Hurricane Katrina (2005) in the turbulent gray zone. *Journal of Advances in Modeling Earth Systems* 7(1):142–161
- Grønnegaard Pedersen J, Kelly M, Gryning SE, Brümmmer B (2013) The effect of unsteady and baroclinic forcing on predicted wind profiles in large eddy simulations: Two case studies of the daytime atmospheric boundary layer. *Meteorologische Zeitschrift* 22(6):661–674
- Hacker J, Draper C, Madaus L (2018) Challenges and opportunities for data assimilation in mountainous environments. *Atmosphere* 9(4):127
- Holton J (1992) *An Introduction to Dynamic Meteorology*. Academic Press
- Jackson P, Hunt J (1975) Turbulent wind flow over a low hill. *Quarterly Journal of the Royal Meteorological Society* 101(430):929–955
- Jacobson M (2005) *Fundamentals of Atmospheric Modeling*. Cambridge University Press
- Jiménez-Esteve B, Udina M, Soler M, Pepin N, Miró J (2018) Land use and topography influence in a complex terrain area: A high resolution mesoscale modelling study over the eastern pyrenees using the WRF model. *Atmospheric Research* 202:49–62
- Kosović B, Curry JA (2000) A large eddy simulation study of a quasi-steady, stably stratified atmospheric boundary layer. *Journal of the Atmospheric Sciences* 57(8):1052–1068
- Kundu P, Cohen I, Hu H (2001) *Fluid Mechanics*. Elsevier Science
- Launder B, Spalding D (1974) The numerical computation of turbulent flows. *Computer Methods in Applied Mechanics and Engineering* 3:269–289
- Lilly K (1966) The representation of small-scale turbulence in numerical simulation experiments
- Liu Y, Warner TT, Astling EG, Bowers JF, Davis CA, Halvorson SF, Rife DL, Sheu RS, Swerdrup SP, Xu M (2008a) The operational mesogamma-scale analysis and forecast system of the u.s. army test and evaluation command. part ii: Interrange comparison of the accuracy of model analyses and forecasts. *Journal of Applied Meteorology and Climatology* 47(4):1093–1104
- Liu Y, Warner TT, Bowers JF, Carson LP, Chen F, Clough CA, Davis CA, Egeland CH, Halvorson SF, Huck TW, Lachapelle L, Malone RE, Rife DL, Sheu RS, Swerdrup SP, Weingarten DS (2008b) The operational mesogamma-scale analysis and forecast system of the u.s. army test and evaluation command. part i: Overview of the modeling system, the forecast products, and how the products are used. *Journal of Applied Meteorology and Climatology* 47(4):1077–1092
- Mason P, Sykes R (1979) Flow over an isolated hill of moderate slope. *Quarterly Journal of the Royal Meteorological Society* 105(444):383–395
- Mathieu J, Scott J (2000) *An Introduction to Turbulent Flow*. Cambridge University Press
- Meij AD, Vinuesa J (2014) Impact of SRTM and corine land cover data on meteorological parameters using WRF. *Atmospheric Research* 143:351–370
- Meneveau C (2019) Big wind power: Seven questions for turbulence research. *Journal of Turbulence* 20(1):2–20

- Mirocha JD, Lundquist JK, Chow FK, Kosovic B (????) New large eddy simulation subfilter turbulence models implemented into the advanced research WRF version 3.0
- Mirocha JD, Lundquist JK, Kosović B (2010) Implementation of a nonlinear subfilter turbulence stress model for large-eddy simulation in the advanced research WRF model. *Monthly Weather Review* 138(11):4212–4228
- Moeng CH, Dudhia J, Klemp J, Sullivan P (2007) Examining two-way grid nesting for large eddy simulation of the PBL using the WRF model. *Monthly Weather Review* 135(6):2295–2311
- Montornes A, Casso P, Lizcano G, Kosovic B (2017) WRF-LES in 250+ real sites: Learnings and challenges. 18th Annual WRF User's Workshop
- Morton D, Molders N (2007) Tradeoffs in resolution versus computational resources in modelling a tanana valley wind event. In: The Great Alaska Weather Modeling Symposium
- Muñoz-Esparza D, Kosović B, Mirocha J, van Beeck J (2014) Bridging the transition from mesoscale to microscale turbulence in numerical weather prediction models. *Boundary-Layer Meteorology* 153(3):409–440
- Pedersen JG, Kelly M, Gryning SE, Brümmer B (2013) The effect of unsteady and baroclinic forcing on predicted wind profiles in large eddy simulations: Two case studies of the daytime atmospheric boundary layer. *Meteorologische Zeitschrift* 22(6):661–674
- Peña A, Floors R, Gryning SE (2013) The Høvsøre tall wind-profile experiment: A description of wind profile observations in the atmospheric boundary layer. *Boundary-Layer Meteorology* 150(1):69–89
- Peña A, Floors R, Sathe A, Gryning SE, Wagner R, Courtney MS, Larsén XG, Hahmann AN, Hasager CB (2015) Ten years of boundary-layer and wind-power meteorology at Høvsøre, denmark. *Boundary-Layer Meteorology* 158(1):1–26
- Pineda N, Jorba O, Jorge J, Baldasano JM (2004) Using NOAA AVHRR and SPOT VGT data to estimate surface parameters: application to a mesoscale meteorological model. *International Journal of Remote Sensing* 25(1):129–143
- Pope S (2000) *Turbulent Flows*. Cambridge University Press
- Porte-Agél F, Meneveau C, Parlange MB (2000) A scale-dependent dynamic model for large-eddy simulation: application to a neutral atmospheric boundary layer. *Journal of Fluid Mechanics* 415:261–284
- Reen BP, Stauffer DR (2010) Data assimilation strategies in the planetary boundary layer. *Boundary-layer meteorology* 137(2):237–269
- Rodrigo JS, Allaerts D, Avila M, Barcons J, Cavar D, Arroyo RC, Churchfield M, Kosovic B, Lundquist J, Meyers J, Esparza DM, Palma J, Tomaszewski J, Troldborg N, van der Laan M, Rodrigues CV (2017) Results of the GABLS3 diurnal-cycle benchmark for wind energy applications. *Journal of Physics: Conference Series* 854:012037
- Schicker I, Arnold Arias D, Seibert P (2016) Influences of updated land-use datasets on WRF simulations for two austrian regions. *Meteorology and Atmospheric Physics* 128(3):279–301
- Skamarock W, Klemp J, Dudhia J, Gill D, Barker D, Wang W, Huang XY, Duda M (2008) A description of the advanced research WRF version 3
- Smagorinsky J (1963) General circulation experiments with the primitive equations. *Monthly Weather Review* 91(3):99–164
- Smith DA, Harris M, Coffey AS, Mikkelsen T, Jørgensen HE, Mann J, Danielian R (2006) Wind lidar evaluation at the danish wind test site in Høvsøre. *Wind Energy: An International Journal for Progress and Applications in Wind Power Conversion Technology* 9(1-2):87–93

- Stauffer DR, Seaman NL, Binkowski FS (1991) Use of four-dimensional data assimilation in a limited-area mesoscale model part ii: Effects of data assimilation within the planetary boundary layer. *Monthly Weather Review* 119(3):734–754
- Steppeler J, Bitzer HW, Minotte M, Bonaventura L (2002) Nonhydrostatic atmospheric modeling using azimuthal coordinate representation. *Monthly Weather Review* 130(8):2143–2149
- Stevens E, Songster K, Morotn D (2010) Using wrf to simulate the saint lawrence island wind storm of february 27, 2009. In: *Alaska Weather Symposium*
- Stevens RJAM, Wilczek M, Meneveau C (2014) Large-eddy simulation study of the logarithmic law for second- and higher-order moments in turbulent wall-bounded flow. *Journal of Fluid Mechanics* 757:888–907
- Stocker TF, Qin D, Plattner GK, Tignor M, Allen SK, Boschung J, Nauels A, Xia Y, Bex V, Midgley PM, et al. (2013) Climate change 2013: The physical science basis
- Stull R (1988) *An Introduction to Boundary Layer Meteorology*. Springer Netherlands
- Talbot C, Bou-Zeid E, Smith J (2012) Nested mesoscale large-eddy simulations with WRF: Performance in real test cases. *Journal of Hydrometeorology* 13(5):1421–1441
- Taylor P (1977) Some numerical studies of surface boundary-layer flow above gentle topography. *Boundary-Layer Meteorology* 11(4):439–465
- Torrecillas AM, Casso P, Lizcano G, Kosovic B (2016) WRF-LES in the real world: Towards a seamless modeling chain for wind industry applications
- Tran T, Tran H, Mansfield M, Lyman S, Crosman E (2018) Four dimensional data assimilation (FDDA) impacts on WRF performance in simulating inversion layer structure and distributions of CMAQ-simulated winter ozone concentrations in uintah basin. *Atmospheric environment* 177:75–92
- Wan F, Porté-Agel F, Stoll R (2007) Evaluation of dynamic subgrid-scale models in large-eddy simulations of neutral turbulent flow over a two-dimensional sinusoidal hill. *Atmospheric Environment* 41(13):2719–2728
- Warner T (2010) *Numerical Weather and Climate Prediction*. Cambridge University Press
- Wilks DS (2011) *Statistical methods in the atmospheric sciences*, vol 100. Academic press
- WRF Community (2000) Weather research and forecasting (WRF) model
- Wyngaard JC (2004) Toward numerical modeling in the “Terra Incognita”. *Journal of the Atmospheric Sciences* 61(14):1816–1826
- Yamaguchi T, Feingold G (2012) Large-eddy simulation of cloudy boundary layer with the advanced research WRF model. *Journal of Advances in Modeling Earth Systems* 4(3)
- Yamazaki H, Satomura T (2010) Nonhydrostatic atmospheric modeling using a combined cartesian grid. *Monthly Weather Review* 138(10):3932–3945
- Yamazaki H, Satomura T (2012) Non-hydrostatic atmospheric cut cell model on a block-structured mesh. *Atmospheric Science Letters* 13(1):29–35